The Extracellular Region of the Receptor for Advanced Glycation End Products Is Composed of Two Independent Structural Units †

6 AUTHORS, INCLUDING:

Guenter Fritz
Universitätsklinikum Freiburg
94 PUBLICATIONS **3,015** CITATIONS

SEE PROFILE

Estelle Leclerc
North Dakota State University
53 PUBLICATIONS **2,431** CITATIONS

SEE PROFILE

Claus W Heizmann
441 PUBLICATIONS **20,526** CITATIONS

SEE PROFILE

Walter J Chazin
Vanderbilt University
282 PUBLICATIONS **9,873** CITATIONS

SEE PROFILE

The Extracellular Region of the Receptor for Advanced Glycation End Products is Comprised of Two Independent Structural Units†

Brian M. Dattilo‡, Günter Fritz§, Estelle Leclerc‖, Craig W. Vander Kooi‡,⊥, Claus W. Heizmann@, and Walter J. Chazin‡,#,*

‡ *Department of Biochemistry, Center for Structural Biology, 465 21st Ave S., 5140 BIOSCI/MRBIII, Vanderbilt University, Nashville, TN 37121-8725*

§ *Department of Biology, University of Konstanz, Universitätsstrasse 10, 78457 Konstanz, Germany*

‖ *Department of Chemistry and Biochemistry, Florida Atlantic University, 770 Glades Road, Boca Raton, FL 33431*

@ *Division of Clinical Chemistry, Children's Hospital, Steinwiesstrasse 75 Zürich, CH 8032*

Departments of Chemistry and Physics, Vanderbilt University

Abstract

The receptor for advanced glycation end products (RAGE) is an important cell surface receptor being pursued as a therapeutic target because it has been implicated in complications arising from diabetes and chronic inflammatory conditions. RAGE is a single membrane spanning receptor containing a very small ~40 residue cytosolic domain and a large extracellular region comprised of 3 Ig-like domains. In this study, high level bacterial expression systems and purification protocols were generated for the extracellular region of RAGE (sRAGE) and the five permutations of single and tandem domain constructs to enable biophysical and structural characterization of its tertiary and quaternary structure. The structure and stability of each of these six protein constructs was assayed by biochemical methods including limited proteolysis, dynamic light scattering, CD, and NMR. A homology model of sRAGE was constructed to aid in the interpretation of the experimental data. Our results show that the V and C1 domains are not independent domains, but rather form an integrated structural unit. In contrast, C2 is attached to VC1 by a flexible linker and is fully independent. The interaction with a known RAGE ligand, Ca^{2+}-S100B, was mapped to VC1, with the major contribution from the V domain but clearly defined secondary effects from the C1 domain. The implications of these results are discussed with respect to models for RAGE signaling.

The receptor for advanced glycation end products (RAGE)[1] is a member of the immunoglobulin (Ig) super-family of cell surface receptors (1,2). RAGE stimulates physiological and pathological effects through interaction with a diverse set of ligands including advanced glycation end products (AGEs) (3–7), amyloid-fibrils (8–10), amphoterin (HMG1) (11), and members of the S100 protein family (12–14). The soluble extracellular

* Address correspondence to this author. Tel: 615-936-2210. Fax: 615-936-2211. E-mail: walter.chazin@vanderbilt.edu.
⊥ current address: Department of Biophysics and Biophysical Chemistry, Johns Hopkins University School of Medicine, 725 N Wolfe St, Baltimore, MD 21205

[1] Abbreviations: RAGE, receptor for AGE; AGE, advanced glycation end products; sRAGE, soluble RAGE; Ig, immunoglobulin; V-type, variable type; C-type, constant type; HMG1, high mobility group box 1

portion of RAGE (sRAGE) is present in human serum, although its specific biological function is under debate (15,16).

The ligand promiscuity of RAGE is provocative, implying a range of potential effects on human health (17,18). AGEs lead to oxidative stress and complications of diabetes such as cardiovascular disease and blindness (19). Amyloid-β peptide leads to neurotoxicity associated with Alzheimer's disease (5). Amphoterin and many S100 proteins act as cytokines when secreted from the cell (20–22). Specifically, S100B, S100A1, and amphoterin exhibit RAGE-dependent trophic effects on neurons at nanomolar concentrations but cause toxic effects at micromolar concentrations (23). Amphoterin stimulation of RAGE also leads to tumor growth and metastasis (24). S100A12 induces both acute and chronic inflammation through its binding to RAGE (12). Remarkably, treatment with exogenous sRAGE has been shown to suppress the acceleration of diabetic atherosclerosis in diabetic murine models (25). The association with specific disease conditions has prompted great interest in RAGE as a therapeutic target (26–28).

Our laboratory is interested in the function of S100 proteins as RAGE ligands. These EF-hand Ca^{2+}-binding proteins are best known as mediators of intracellular Ca^{2+} signals, although they are also exported from the cell by a yet unknown mechanism (29). S100 proteins have an exposed hydrophobic binding pocket that mediates protein-protein interactions (30–32). Additionally, all S100 proteins are minimally homodimeric but some heterodimerize (33) and many appear to form higher order homo- and hetero-oligomers (34,35).

Oligomerization is a common mechanism for activation of a cell surface receptor and many Ig-like proteins are known to oligomerize (36). However, analytical ultracentrifugation has been used to show that bacterially expressed sRAGE is monomeric (37). The lack of intrinsic sRAGE oligomerization is consistent with the initial purification of RAGE (2) and has been corroborated by studies with mouse RAGE and recombinant sRAGE from yeast (38,39). Although these studies all point to monomeric sRAGE, it should be noted that no information exists on the oligomeric state of the intact receptor in a membrane environment. The identification of S100 protein as RAGE ligands is intriguing in this context, as these may provide a means for ligand-induced receptor oligomerization.

Knowledge of the structure of RAGE is important for understanding how it is activated and functions in cellular signaling. RAGE is composed of a large extracellular ligand-binding region with three Ig-like domains (one V-type and two C-type, assigned based on sequence homology), a short transmembrane helix, and a highly acidic intracellular domain essential for RAGE signaling (40). Structures of Ig-like domains reveal predominately β-sheet secondary structure folded into a two sheet β-sandwich and are classified according to the number and organization of β-strands (41). A conserved pair of cysteines, which form a disulfide bond between the two sheets, is frequently present in Ig-like domains.

Understanding the structural organization of RAGE and receptor-ligand interactions is a necessary step towards elucidating the molecular basis for RAGE function. In this study we focus on characterizing the structure of sRAGE and its interactions with an S100 protein ligand, S100B, using a variety of biochemical and structural methods. A series of sRAGE constructs were prepared and used to characterize its structure and interactions with a specific S100 protein ligand, S100B. In addition, a structural model for sRAGE was constructed to aid in the interpretation of the data in terms of models for RAGE signaling.

MATERIALS AND METHODS

Molecular Biology

Bacterial expression vectors for human sRAGE (GenBank accession no. NM_001136) and its five single and tandem domain fragments (V, C1, C2, VC1, C1C2) were all produced by three steps. DNA was extracted from baculovirus-infected insect cells generously provided by Dr. Ann Marie Schmidt (Columbia University, New York, NY). DNA fragments were PCR amplified with primers containing 5′ NdeI and 3′ XhoI (containing the stop codon) restriction sites and contained the following RAGE protein sequences excluding the 22 amino acid signal peptide: sRAGE (23–327), VC1 (23–243), C1C2 (122–327), V (23–132), C1 (122–243), C2 (235–327). DNA fragments were subcloned into the NdeI and XhoI sites of pET15b vector (Novagen), which produced N-terminal His_6 tagged fusion proteins separated by a thrombin cleavage site. Creation of a human S100B expression vector in pGEMEX, which produced protein of wild-type sequence, was described previously (42). Three Cys → Ser mutants of human S100B (C84S, C68S, C68S/C84S) were produced in the pGEMEX expression vector using the QuickChange strategy (Strategene).

Protein Expression and Purification

RAGE fragments were overexpressed in *Escherichia coli* strain OrigamiB(DE3) (Novagen) grown at 37 °C to OD_{600} ~0.8, adjusted to 20°C for 30 minutes, induced with 0.5 mM IPTG, and allowed to express for 4–6 hours. Cells were lysed at 4 °C in 20 mM Tris-HCl, 20 mM imidazole, 300 mM NaCl at pH 8.0 in the presence of lysozyme (5mg/ml), followed by sonication (5 min with a 50% duty cycle). Clarified lysate was initially purified on His-Select (Sigma) resin equilibrated in the lysis buffer and eluted with a 4 column volume (CV) linear gradient to 20 mM Tris-HCl, 300 mM imidazole, 300 mM NaCl at pH 8.0. Following dialysis, the His_6 tag was removed by thrombin cleavage (1–2 units per mg of protein) incubated at room temperature for 1–2 hours followed by separation over SourceQ (C2) using 20 mM Tris-HCl at pH 7.7 and a 18 CV linear gradient from 0 to 1 M NaCl or MonoS (sRAGE, VC1, C1C2, V, C1) using 20 mM sodium phosphate at pH 6.0 and a 18 CV linear gradient from 150 to 850 mM NaCl (GE Healthcare). The His_6 tag was not cleaved from C1 or C1C2 due to observation of secondary cleavage. The amino acids Gly-Ser-His-Met remained at the N-terminus after thrombin cleavage.

The expression system for human S100B in pGEMEX vector was described previously (42) except luria broth (LB) was used in place of DYT. Cells were resuspended in 20 mM Tris-HCl at pH 7.7 and lysed at 4 °C in the presence of lysozyme (5mg/ml) followed by sonication (5 min with a 50% duty cycle). Purification of samples involved an initial step of DEAE ion exchange chromatography, equilibrated in 20 mM Tris-HCl at pH 7.7 and eluting bound protein using a linear gradient from 0 to 1 M NaCl. This was followed by Superdex 75 gel filtration in 20 mM Tris-HCl, 0.1 mM EDTA at pH 7.7. C84S, C68S, and a double C68S/C84S mutant of S100B were purified the same as wild-type.

Samples of ^{15}N-enriched sRAGE and S100B proteins were produced as described above except for the use of M9 minimal media containing $^{15}NH_4Cl$ as the sole nitrogen source. $^2H,^{15}N$-enriched protein (~85% as estimated by MALDI mass spectrometry) was produced in a similar manner using cells adapted to growth in ^2H_2O. The integrity of each protein sample was verified by SDS-PAGE and MALDI mass spectrometry.

Limited Proteolysis/Protease Protection

Limited proteolysis was performed at room temperature on sRAGE and domain fragments that had been dialyzed against 10 mM HEPES-NaOH, 75 mM NaCl at pH 7.0. Typically, 50–100 µg of purified protein were incubated with trypsin at an enzyme to protein ratio of 1:500 (w/

w) and a volume of 100 μl. The reaction was stopped at various time points by mixing 14 μl of reaction mix with 14 μl 2× SDS loading buffer and heating at 90 °C for 5 minutes. For protection assays, S100B was mixed with sRAGE or domain fragments at a 2:1 molar stoichiometry of RAGE to S100B dimer, anticipating two binding sites per S100B dimer. $CaCl_2$ was added to a final concentration of 1 mM prior to the addition of enzyme. Control experiments with S100B alone and sRAGE or domain fragments were performed under identical conditions (i.e. in the presence of Ca^{2+}).

Mass Spectrometry

Matrix-assisted laser desorption/ionization time-of-flight mass spectrometry (MALDI-TOF MS) analysis was performed on tryptic peptides derived from gel-excised Coomassie stained bands. Samples were prepared by the dried-droplet method using β-cyano-4-hydroxycinnamic acid [dissolved in water/acetonitrile/trifluoroacetic acid (39.2:60:0.1) at a concentration of 5 mg/mL, supplemented with 1 mg/mL ammonium citrate] as a matrix. The peptides were initially identified by comparing the experimental masses of each peak with computer-predicted masses of tryptic peptides from the RAGE sequence. Amino acid sequence identity was definitively established by inducing ion fragmentation using tandem TOF-TOF MS.

CD

All samples were buffer exchanged into 50 mM potassium phosphate at pH 7.5. Protein concentration was typically around 30 μM. Data ranging from 200–240 nm (1 nm increment) were acquired on a Jasco J-810 CD spectrophotometer (Easton, MD). Baseline was adjusted during acquisition from data acquired on the solution alone. All data were converted to mean residue ellipticity using the following equation:

$$[\Theta] = 100 * signal/C\,n\,1$$

(1)

where $[\Theta]$ is mean residue ellipticity in units $deg \cdot cm^2 \cdot dmol^{-1}$, signal is the raw signal output in mdeg, C is protein concentration in millimolar, n is the number of residues, and l is the cell pathlength in centimeters. Fitting using the K2d web server was used to estimate secondary structure content (43).

Dynamic Light Scattering

All data were acquired using a DynaPro ProteinSolutions molecular sizing instrument (Wyatt Technology Corporation). Typically, 150 μM protein in 10 mM HEPES-NaOH, 75 mM NaCl at pH 7.0 in a volume of 60 μL were filtered and centrifuged at $>15,000 \times g$ to remove any particulate matter. Twenty scans were accumulated for each sample at room temperature. The data were analyzed using the Dynamics 5 software provided by the manufacturer and are represented as mean radius ± polydispersity.

Differential Scanning Calorimetry

Samples of sRAGE, VC1, C1C2, V, C1, and C2 (50–100 μM) were buffer exchanged into 50 mM sodium citrate at pH 6.7 using a 50 mL desalting column (GE Healthcare) to ensure identically matched buffer components. Data were collected on a VP-DSC (Microcal; Northampton, MA) with a scan from 20 °C to 100 °C at a rate of 90 °C/hr. 50 mM sodium citrate at pH 6.7 was used as the reference solution. All samples and buffers were thoroughly filtered and degassed prior to analysis. Data were analyzed using the Origin7 software package provided by the manufacturer, baseline corrected for buffer alone, and fit with a non 2-state equation.

Surface Plasmon Resonance

CM5 sensor chips, coupling reagents (NHS, EDC and ethanolamine), and P20 were purchased from Biacore International SA (Freiburg, Germany). CM5 sensor chips were preactivated using the NHS:EDC chemistry according to previously published procedures (44,45). 50 μg/ml V, VC1, C2, or yeast sRAGE in sodium acetate buffer at pH 5.5 was injected over the preactivated surface in order to obtain about 5000 RU. The surface was then blocked with ethanolamine. In each experiment, the fourth flow-cell of the sensor chip was kept empty and used as an internal reference. A series of various concentrations, ranging from 12.6 μM to 1.57 μM for S100B, were injected over the flow-cells. The running buffer was 50 mM Tris-HCl, 150 mM NaCl, 5 mM $CaCl_2$, 0.005% P20 at pH 7.4. The surface was regenerated each time by 1 min contact with 0.5 M EDTA following by 1 min contact with 50 mM borate, 1M NaCl at pH 8.5.

Binding data were analyzed by global analysis using BiaEvaluation 3.1 software from the manufacturer (Biacore), in which association and dissociation data for the series of S100B concentrations were fitted simultaneously (46).

NMR

Standard ^{15}N-^{1}H HSQC and TROSY-HSQC (47) spectra were acquired at 298 K on Bruker *Avance* 600 and 800 MHz spectrometers equipped with triple resonance cryoprobes. Typical acquisition parameters were 128 scans with 1024 points in the direct (^{1}H) dimension and 128 points in the indirect (^{15}N) dimension. Fourier transform, zero filling, and a 90 degree shifted squared sine window function were applied using XWINNMR (Bruker) and analyzed using Xeasy (48). The spectrum for sRAGE was obtained in a solution containing 200 μM protein in 20 mM sodium phosphate, 250 mM NaCl at pH 6.0. Initial spectra for the other constructs were obtained under these conditions, and then optimized specifically for each. Deviations from the sRAGE conditions were: V, 10 mM sodium citrate at pH 6.0; C2, 20 mM sodium phosphate at pH 6.0. Protein concentrations were determined using the UV absorbance at 280 nm under denaturing and reducing conditions and ranged from 200 to 500 μM.

For studying sRAGE-S100B interactions, ^{15}N-V and unlabeled S100 proteins were buffered in 10 mM HEPES-NaOH at pH 7.0, 75 mM NaCl and 10 mM $CaCl_2$. Spectra of isolated proteins and protein-protein complexes were acquired under identical conditions with a 2:1 ratio of RAGE to S100B dimer. Samples of $^{2}H,^{15}N$-sRAGE were buffer exchanged into 20 mM sodium phosphate and 500 mM NaCl at pH 6.0 in 100% H_2O. Sample volume was ~160 μL in a 3 mm NMR tube, which was placed within a 5 mm NMR tube filled with >99.9% $^{2}H_2O$.

Homology Modeling

Sequences for human sRAGE and domain constructs were submitted to the ESyPred3D web server (49). The program performs all steps of homology modeling including homolog identification (PSI-BLAST of NCBI NR databank then scored against the PDB), multiple sequence and pairwise alignments (combination of ClustalW, Dialign2, Match-Box, Multalin, and PRRP), and model building (MODELLER). Models were generated using the following proteins: VC1, Fab light chain in complex with human factor 8 (PDB 1IQD); V, mouse junction adhesion molecule (PDB 1F97); C1, human B7-1 (PDB 1DR9); C2, human APEP-1 (PDB 1U2H). Side chains were repacked and energy minimized using SCWRL 3.0 (50). PROCHECK was used to assess the stereochemical properties of each model (51). To analyze the surface area buried in the V-C1 contacts, the model was split after the linker. Fast Connolly surfaces were generated in the program Sybyl (Tripos) for the full VC1 model (25–222), V domain (25–121), and C1 domain (122–222).

RESULTS

Production of sRAGE and domain constructs

High level production and purification protocols were developed for sRAGE and the five single and tandem domain constructs (VC1, C1C2, V, C1, C2; see Figure 1A). While the production of recombinant sRAGE has been described for both eukaryotic and prokaryotic expression systems (12, 37, 39, 52), the strategy described here provided consistent high level production of all six constructs without the need to refold protein from inclusion bodies. Bacterial expression vectors were constructed that enable purification via an N-terminal His_6-tag and Ni^{2+} affinity chromatography. Use of cells providing an oxidizing environment and optimization of expression parameters (temperature, duration, IPTG concentration) produced soluble protein for each of the constructs. Protein yields after purification were similar for sRAGE, VC1, V, and C2 (15–20 mg/L) and lower for C1C2 and C1 (5–10 mg/L) as a result of their lower expression levels.

When performing structural analysis on isolated domains of a protein, it is important to properly define construct boundaries. Initial boundaries were based on sequence alignment with known Ig family sequences and secondary structure prediction. Ala23 represents the first amino acid of the native receptor after loss of the signaling peptide and was selected as the N-terminus for our sRAGE construct. The C-terminus of sRAGE, Gly327, represents the end of the C2 structural region, which is linked to the transmembrane helix. The N-terminus for the V and VC1 constructs and the C-terminus for the C1C2 and C2 constructs were the same as for sRAGE. The predicted linker region separating C1 and C2 was identified by multiple sequence alignments of four RAGE genes (human, bovine, rat, and mouse; Figure S1 in Supporting Information). The eleven amino acid insert in bovine RAGE after Trp230 aided identification since regions of low identity and homology often represent loop and linker regions. The intervening boundaries between V and C1 proved to be more challenging to precisely identify and had to be manually optimized based on expression level, solubility, and stability. This analysis suggests there may be unique features relating V to C1.

Analysis of purified constructs under reducing and non-reducing SDS-PAGE conditions showed a mobility shift consistent with formation of disulfide bonds (Figure S2). Observing a single band under non-reducing conditions suggested homogeneity in disulfide formation. Interestingly, ^{15}N-^1H HSQC spectra of V acquired in the presence of reducing agent showed a collapse of the chemical shift dispersion in the ^1H dimension, which is characteristic of an unfolded protein (Figure S3). This suggests any experiments in the presence of reducing agents could lead to artifacts due to protein unfolding.

Stability of sRAGE domains

A series of limited proteolysis experiments were performed in order to further characterize the domain structure of sRAGE. A time course for digestion of the protein by trypsin shows that sRAGE is completely digested within four hours (Figure 1B). Two major species are formed during early time points, one migrating at ~25 kDa (Figure 1B, arrow b) and another at ~12 kDa (Figure 1B, arrow c). In-gel digestion of the 25 kDa band with trypsin followed by MALDI-MS analysis showed this band contained peptides unique to the V and C1 domains. Figure 1C shows the sequence coverage obtained for both intact sRAGE (Figure 1B, arrow a) and the ~25 kDa fragment. Notably, coverage obtained for the V and C1 domains was nearly complete in the 25 kDa band (Figure 1B, arrow b), ranging from a peptide encoding a region of the N-terminus (23–29) to a peptide near the C-terminus of C1 (199–216).

To further confirm the origin of the 25 kDa band, limited proteolysis of VC1 (Figure 1D) was performed under conditions identical to those used for sRAGE. Digestion of VC1 produced a

small truncation to a band with the same mobility as the 25 kDa band generated from sRAGE digestion (arrow d, Figure 1D). Both the intact VC1 and the 25 kDa fragment were digested at the same rates as those observed in the experiment with sRAGE. Notably, the 25 kDa fragment produced from either sRAGE or VC1 digestion was largely stable to further proteolysis despite the presence of both lysine and arginine residues in the expected linker region between the two domains. To further understand the apparent stability of the V-C1 linker we performed limited proteolysis experiments on isolated V and C1. Figure 1D shows that both intact V and especially C1 were much more susceptible to trypsin proteolysis than the 25 kDa fragment that contained both V and C1. Furthermore, we failed to observe a truncation to a stable fragment for either construct that would indicate the presence of a single stable V or C1 domain.

Unlike sRAGE and VC1, the C1C2 construct was completely digested by trypsin in 5 minutes, and only a single 12 kDa band was observed thereafter (Figure S4). This stable band had identical mobility to the 12 kDa band seen in the sRAGE digestion (Figure 1B, arrow c). The presence of this band in sRAGE and C1C2 digestions, but not for VC1, implies the band belongs to the C2 domain. Exposure of isolated C2 to trypsin showed it is completely stable to digestion by this protease (Figure S4). This observation is identical to that made for the 12 kDa band in the sRAGE (Figure 1B, arrow c) and C1C2 digestions. The assignment of the 12 kDa band to C2 and the absence of other bands in C1C2 digestions indicate that the C1 domain on its own is not stable.

Differential scanning calorimetry (DSC) experiments were performed to better understand the stability and interdependence of sRAGE domains. Intact sRAGE showed a single thermal transition with a T_m at 55.1 °C, which was surprising given the much higher T_m value of isolated RAGE C2 (vide infra). Unfortunately, heating beyond 60 °C leads to aggregation and precipitation (Figure 2, solid line), which precludes further analysis. VC1 responded in a very similar manner, with a single transition corresponding to T_m at 55.1 °C followed by aggregation and precipitation (Figure 2, dashed line). In an attempt to determine if the thermal transition derives specifically from one domain, DSC experiments were performed on isolated V and C1. However, although the proteins remained soluble, no discrete transitions were observed for either of the isolated domains (Figure S5). These observations were consistent with the limited proteolysis experiments, which suggested that isolated V and C1 were not stably folded independent domains. Based on the evidence from the thermal denaturation and limited proteolysis data, we attribute the unfolding event at 55 °C to uncoupling of the V and C1 domains. Remarkable parallels are found in a very thorough study of the unfolding of a tandem (one V-type and one C-type domain) Ig protein from a multiple myeloma κI light chain, from which the authors concluded that the phenomena observed did not correspond to unfolding of independent structural domains (53).

Analysis of C1C2 and C2 constructs showed a single unfolding transition with T_m values of 72.7 °C and 74.3 °C (Figure S6; Figure 2, dotted line), respectively. In both cases this transition was nearly 100% reversible. This distinct thermal transition is attributable to unfolding of the C2 domain, which supports our limited proteolysis data suggesting that C2 is independent from the rest of the sRAGE molecule. We note that the unfolding transition for C2 in the context of full sRAGE was not observed because it was masked by the aggregation/precipitation associated with VC1 that occurs well below the T_m of C2. Taken together, the limited proteolysis and DSC data imply that the three predicted domains are present. However, whereas C2 is a completely independent and highly stable domain, V and C1 are seen to have a significant influence on each other's stability.

sRAGE is composed of coupled V and C1 domains with an independent C2

Circular dichroism and NMR were used to characterize the secondary and tertiary structure of sRAGE. CD provided distributions of secondary structure elements for each of the six protein constructs, all of which showed a combination of β-sheet and random coil. Remarkably, sRAGE, VC1, C1C2, and C2 all were assigned 47% β-sheet, 48% random coil, and 5% α-helix, and only slightly reduced β-sheet and increased random coil was observed for isolated V (40% β-sheet, 51% coil) and C1 (43% β-sheet, 48% coil). These results show all six protein constructs contain secondary structure highly consistent with one or more Ig-like folds.

The tertiary structure of sRAGE and each of the tandem and single domain constructs was analyzed by ^{15}N-^{1}H HSQC NMR (Figure 3). Despite the relatively small size of the three domains, it was surprisingly difficult to obtain high quality NMR spectra. Experimental conditions (temperature, pH, and ionic strength) for each construct had to be optimized independently. Dynamic light scattering was also used to complement the NMR experiments, in particular to assess the whether the domain constructs were monomeric under the conditions of the NMR experiments. Hence, the light scattering data were collected at the same protein concentrations as those used in NMR experiments.

In the ^{15}N-^{1}H HSQC spectrum of sRAGE, less than 100 crosspeaks were observed (Figure 3A). The linewidths of these signals were relatively narrow, as would be expected for a single Ig domain. Moreover, the signals correspond precisely to the peaks observed in the corresponding spectrum of isolated C2 (Figure 3F). Since the NMR chemical shift is an exquisitely sensitive probe of structure, these observations indicate that the observed peaks in the sRAGE spectrum arise from C2. Of note, signals in both spectra have uniform intensity and line width and are well dispersed, consistent with a well-folded globular domain. In addition, light scattering data on isolated C2 were fit to a mean radius of 2.21 ± 0.27 nm with a polydispersity of 12%, fully consistent with a monomeric non-spherical β-sandwich.

Why are the V and C1 peaks from sRAGE so much broader than the C2 peaks that they are not observed in a standard HSQC spectrum? Since previously published analytical ultracentrifugation experiments showed that sRAGE is monomeric (37), the likely explanations are the two domains tumble in solution with the characteristics of a larger particle or that they are both conformationally heterogeneous. To obtain further insight, light scattering experiments were performed on sRAGE to verify that the protein is monodisperse. Unfortunately, the data were ambiguous because the level of polydispersity assigned (33.5%) is above the threshold for which reliable conclusions can be drawn. [We believe sRAGE is not poly-disperse, but rather that the fitting of light scattering data is not straightforward because sRAGE contains two independent, flexibly linked structural modules.] We therefore turned to the smaller VC1, V and C1 constructs to obtain further insights.

The ^{15}N-^{1}H HSQC spectrum of VC1 showed at least 150 distinct backbone peaks out of a maximum of ~200 (Figure 3B), as expected for a protein of this size. Not every peak will be discernable in a 2D experiment because those in the crowded central region are likely to overlap. Importantly, the relatively sharp and well dispersed peaks from C2 observed in the spectrum of sRAGE were clearly not present in the spectrum of VC1. Moreover, the linewidths of the peaks in the VC1 spectrum were significantly larger than those observed for the C2 domain in the spectrum of sRAGE. Light scattering data on VC1 were fit to an average radius of 3.43 ± 0.33 nm with a low level of polydispersity (9.5%). The radius suggests an elongated molecule consistent with the homology model generated for VC1 described below in addition to the ellipsoid structure modeled from analytical ultracentrifugation (37), and indicates that the VC1 protein is monomeric. The ability to observe a rather complete and well-dispersed ^{15}N-^{1}H HSQC spectrum for VC1 with relatively uniform peak intensities, combined with the light scattering analysis and the lack of signals for VC1 residues in the spectrum of

sRAGE, strongly implies that the V and C1 domains are well-folded and suggests that they tumble as an integrated structural unit.

To further verify the conclusions from the analysis of VC1, the use of specialized techniques to improve the sRAGE spectrum including TROSY and perdeuteration of the protein was investigated (47,54). Perdeuteration in particular provided a substantial improvement (Figure 4), and resulted in well over 200 discrete peaks in the spectrum. Interestingly, there are two populations of peaks in spectra of perdeuterated sRAGE with different relative intensities and linewidths. Many peaks from the subset with lower intensity/wider linewidths were well dispersed into both upfield and downfield regions and corresponded well with peaks in the spectrum of VC1 (Figure 4, red circles). The subset with higher intensity/narrower linewidths overlap well with the C2 peaks observed in spectra of protonated sRAGE, C1C2, and C2 (Figure 3A, 3C, 3F, Figure 4, green circles). Together, these observations show that V and C1 are indeed folded in the context of sRAGE and that the lower intensity/wider linewidth peaks in the spectrum of sRAGE arise from these domains. The fact that linewidths of peaks from the V and C1 domains are the same and significantly larger than those of C2 strongly implies that V and C1 form an integrated structural unit.

Further support for the structural integration of the V and C1 domains was obtained from comparisons to the chemical shifts of isolated V and C1 (Figure 3). The ^{15}N-^{1}H HSQC spectrum of C1 is highly heterogeneous, with a large excess of peaks. In addition to a number of well dispersed peaks, a large number of overlapped peaks in the central region are observed along with a significant variation in signal intensity (Figure 3E). Light scattering experiments revealed a very high 39.2% level of polydispersity. These observations are indicative of a meta-stable C1 domain with substantial unfolded or partially folded regions. The ^{15}N-^{1}H HSQC spectrum of isolated V (Figure 3D) has about the expected number of peaks but linewidths are significantly larger than the peaks observed in the spectrum of the well-folded C2 domain. The larger linewidths of V are presumably the result of conformational heterogeneity as observed for C1 or possibly compounded by some self-association, both as a by-product of separation from C1. The high level of polydispersity (34.5%) in light scattering on this domain is consistent with a lack of structural stability and a tendency to aggregate.

Despite the complications of working with the isolated V and C1 domains, detailed comparison of NMR chemical shifts of V, C1 and VC1 could be performed to obtain domain-specific assignments. This was possible because many peaks in the spectrum of VC1 could be assigned to the V or C1 domain since they appeared in a nearly identical and distinctive location in the spectrum of both VC1 and the corresponding isolated domain. In addition to these peaks that correspond very closely, there were a number of characteristic peaks in the spectra of isolated V and C1 that appear in clearly different locations in the spectrum of VC1, as shown in Figure 5. For the V domain, approximately 50 peaks outside the crowded 8.0–8.5 ppm ^{1}H region could be distinguished. Among these, approximately 20 were clearly shifted relative to their position in the spectra of VC1 and sRAGE. A number of readily distinguishable C1 peaks could also be identified, but the analysis was not nearly as complete due to the meta-stability of C1. Regardless, there is sufficient data to conclude that there are perturbations of peaks in the downfield dispersed region, which indicates that the structure of V is altered by the presence of C1 and vice versa, i.e. there is a specific structural interface between V and C1. In conclusion, our data show the V and C1 domains of sRAGE form an integrated structural unit that is structurally independent of and dynamically linked to the C2 domain.

Homology modeling of sRAGE

A homology model of the three-domain sRAGE protein was constructed using MODELLER software via the ESyPred3D web server in order to facilitate analysis of our structural data and better understand the implications for cellular signaling. An extensive database of Ig-like

domain sequences and structures are available, which implied a high quality model could be generated. The automated pairwise alignment module selected NCAM (PDB id 1QZ1) as the template protein because it has 19% identity with sRAGE after alignment. However, the structure of NCAM has no significant linkers between any of the domains, which differs from our analysis of sRAGE. Thus, we decided to generate models of VC1 and C2 separately.

The pairwise alignments against VC1 resulted in highest homology with an Fab light chain (PDB 1IQD), which has 17.6% identity, so this structure was used to generate the model (Figure 6A). Figure 6B shows the final pairwise alignment of VC1 with the template, which reveals that many of the residues involved in inter-domain packing are not conserved. Hence, the intimate details of the interdomain packing and orientation in the model are viewed as an approximation. On the other hand, the global features of the model have a very high likelihood of being accurate. The high quality of the VC1 model is reflected in an analysis with PROCHECK, e.g. 87% of residues are in most favorable conformations, 11% in the additionally allowed region, and 2% in the generously allowed region. Similar high quality results were obtained for the C2 domain, which was modeled from human APEP-1 (PDB 1U2H).

The VC1 homology model predicts globular structure for residues Asn25-Thr222. Thus, in the VC1 construct (Ala23-Glu243) used in our experimental studies, the C-terminal 21 residues are predicted to be unstructured because they span the C1-C2 linker and into the C2 domain. In the model, the linker between V and C1 is predicted to be only three residues in length, Gln119-Pro121, since Tyr118 forms backbone hydrogen bonds to a β-strand in the V domain and Gly122 forms backbone hydrogen bonds to a β-strand in the C1 domain (Figure 6). A critical aspect of the model is that these three linker residues are predicted to contribute to inter-domain packing along with several residues from the V domain (Thr27, Glu94, Arg114, Arg116, Val117, Tyr118) and the C1 domain (Tyr150, Ala152, Arg178, Arg179, Thr183, Gly184, Phe186. The solvent accessible surface of V and C1 that is buried in the VC1 model is ~500 Å^2 in each subunit. Although the relatively small size of this interface suggests that the intrinsic affinity of the two domains is relatively weak, the interaction between the domains will be enforced by the short length and structural integration of the linker. This interpretation is supported by the lack of chemical shift perturbations in NMR experiments acquired for mixtures of isolated V and C1 domains. Thus, the model is fully consistent with our observation that V and C1 have a structural interface and tumble as an integrated structural unit.

S100B binds to the V domain of RAGE with nM affinity

Having established limited proteolysis conditions for sRAGE and the six domain constructs, proteolysis experiments could be used to characterize the interaction of S100B with RAGE. Initial studies with wild-type S100B led to disulfide cross-linking between S100B and the V domain. While the S100B-sRAGE disulfide cross-linking could be reversed by addition of DTT, the reducing agent also caused the cleavage of the disulfide bond essential to maintain the structure of V (Figure S3). Consequently, a series of three Cys → Ser mutants in S100B were prepared (C68S, C84S, C68S/C84S) and purified. Analysis of the V construct in the presence of the three mutants by SDS-PAGE under non-reducing and reducing conditions confirmed that the reactive cysteine was Cys84, so the C84S mutant was used for all further experiments (Figure S7). Notably, this cysteine to serine mutant was shown previously to be functional (55).

Studies of isolated sRAGE showed that trypsin digestion results in complete loss of the intact protein within 4 hours (Figure 1B). The overall rate of digestion was similar in the presence of Ca^{2+}-S100B (Figure 7A), although sRAGE was slightly, yet reproducibly, better protected in the presence of S100B than in isolation. As expected, this observation was dependent on the presence of Ca^{2+}. Interestingly, the 25 kDa band identified as VC1 in the digestion of free

sRAGE was completely absent when Ca^{2+}-S100B was present (Figure 7A, see arrows). This observation was also Ca^{2+}-dependent. While protection from proteolysis is more common, an *increased* rate of proteolysis is also possible when structural perturbations are induced by protein-protein interactions. The expedited degradation of the VC1 fragment in sRAGE digests could not be explained by the presence of a contaminating protease in our S100B sample since this would be inconsistent with the observation that degradation of the intact protein was slowed. Thus, the interaction between Ca^{2+}-S100B and sRAGE appears to cause a conformational change in the VC1 region of sRAGE that enhances proteolysis by trypsin.

To corroborate these findings, the experiments were repeated with the various sRAGE domain constructs. Much like intact sRAGE, isolated VC1 was reproducibly protected in the presence of Ca^{2+}-S100B, but the 25 kDa fragment was very rapidly degraded (Figure 7B). The isolated V domain was also more rapidly degraded in the presence of Ca^{2+}-S100B consistent with the increased rate of proteolysis on VC1 (Figure S8). Corresponding experiments with C1C2 and isolated C1 and C2 revealed no interaction with Ca^{2+}-S100B as the C1 domain continues to be degraded extremely rapidly under all conditions, and the C2 domain remains totally resistant to digestion by trypsin under the conditions of our experiments. Together, these limited proteolysis results indicate that the interaction of S100B with RAGE is Ca^{2+}-dependent and localized primarily to the V domain.

S100B-sRAGE binding was further investigated using NMR spectroscopy. The optimal conditions for acquiring NMR spectra for sRAGE required the use of high ionic strength buffer (>250 mM NaCl). However, the complex could be formed successfully only at lower ionic strength (<100 mM NaCl), conditions under which, remarkably, free sRAGE had only very limited solubility. The fact that binding of S100B solubilized sRAGE is, in and of itself, confirmatory evidence of an interaction between S100B and sRAGE. The ^{15}N-^{1}H HSQC and TROSY-HSQC spectra of ^{2}H,^{15}N-sRAGE in the presence of excess Ca^{2+}-S100B showed only peaks arising from C2. The absence of signals from VC1 is interpreted as a result of binding of S100B to one or both domains, since it is expected that a large molecular complex is formed containing an S100B dimer and presumably two sRAGE molecules, although no conclusive experimental evidence is currently available. The observation of C2 signals, completely unperturbed, indicates that C2 retains its rotational freedom from the rest of the complex.

To complement the study of S100B binding to sRAGE, NMR was used to probe the interaction with the V and VC1 constructs. In titrations of ^{15}N-enriched V and VC1 with Ca^{2+}-S100B, a uniform decrease in signal intensity was observed for all except ten of the crosspeaks in VC1 as S100B was added. The few VC1 signals that remained observable had chemical shifts and linewidths consistent with being part of the flexible, unstructured tail at the C-terminus of this construct. Control experiments on C1C2, C1 and C2 showed no changes in ^{15}N-^{1}H HSQC spectra induced by the presence of Ca^{2+}-S100B. Thus, consistent evidence was obtained for relatively strong interaction of S100B with sRAGE, and that the V domain is clearly involved.

A detailed analysis of surface Plasmon Resonance (SPR) measurements for S100B binding to immobilized sRAGE revealed affinity constants in the nM range (EL, GF, CWH, in preparation). SPR was used here to further probe the binding of S100B to sRAGE using VC1, V and C2 constructs. In these experiments, binding was observed to VC1 and V, but no interaction with the C2 domain was detected.

Typical S100B binding curves for VC1 and V chips are shown in Figure 8. In the case of VC1, the data were fit with the parallel reaction model for heterogeneous ligand:

$$A+B1 \leftrightarrow AB1 \text{ and } A+B2 \leftrightarrow AB2$$
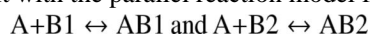
where one analyte molecule (A = S100B) can bind independently to two ligand molecules B1 or B2 (VC1) with K_{D1} the dissociation constant of the first equilibrium, and K_{D2} the corresponding parameter for the second event. This analysis gave two binding constants: $K_{D1} = 11.1$ nM and $K_{D2} = 244$ nM. These results are largely consistent with the affinity determined for intact sRAGE. The S100B binding curves for the V domain (Figure 8B) were also fit with the parallel reaction model. Fitting of the binding data resulted in $K_{D1} = 550$ nM and $K_{D2} = 470$ nM. Although the quality of the fit for K_{D1} was much poorer for VC1 than for the isolated V domain, the affinity of S100B for the immobilized VC1 construct is clearly higher than that for the isolated V-domain. In summary, our data indicate that S100B binds to the V domain of sRAGE and while V contains a site sufficient for binding of S100B dimers, additional contributions are made either directly or allosterically by the C1 domain.

DISCUSSION

The modular structure of sRAGE

The generation of efficient protein expression systems was critical to the studies reported here, and opens the door to use these reagents to probe RAGE function. Our biophysical and structural characterization showed that C2 exhibits the characteristics of a stable well-folded structural domain. In contrast, V and C1 do not form fully independent structural domains but rather behave as a single structural unit. Thus, in the model for the structure of sRAGE, the C2 domain retains significant rotational freedom, whereas V and C1 are structurally inter-dependent.

There is ample evidence for V and C1 forming an integrated structural unit. From the initial stages of analysis, the C1 domain in particular appeared to be rather unstable without V. Many constructs of C1 and C1C2 were designed in the attempt to obtain expression of soluble protein in *E. coli* and it was only after extensive optimization that even limited success was obtained. Even the most stable of the C1 constructs exhibits clear signs of heterogeneity, is digested rapidly in limited proteolysis experiments, and readily degrades over time. The ^{15}N-^{1}H HSQC spectrum of our optimized C1 construct contains some signals with chemical shift dispersion, but the existence of a large excess of peaks with variable intensities and the crowding of many signals in the central region suggests that the isolated domain is structurally heterogeneous and in fact a significant portion of this construct may be unstructured. The isolated V domain is more stable and structured than isolated C1. For example, it was digested more slowly by trypsin and the ^{15}N-^{1}H HSQC spectrum of V has far fewer peaks than C1, although it too shows signs of conformational heterogeneity. Importantly, both the V and C1 domains become significantly more stable to trypsin digestion and more structurally homogeneous when they are linked to each other in the VC1 and sRAGE constructs.

The homology model helps to explain several key experimental observations. For example, the observation of a 2–3 kDa truncation of VC1 in limited proteolysis experiments can be correlated with the prediction of a ~20 residue unstructured C-terminal tail in our RAGE(23–243) VC1 construct. The model also explains the ~10 extremely sharp peaks observed in the HSQC spectrum of V, which the model predicts arise because our V construct (23–132) extends 14 residues beyond the predicted C-terminus of the domain. The NMR signals from these sharp resonances change significantly when they are incorporated into the VC1 construct, which we attribute to their shift from being unstructured in isolated V to participating in β-sheet secondary structure when the C1 domain is included (Figure 5). Our homology model also suggests three large C1 sidechains (Tyr150, Arg179, Phe186) with significant hydrophobic character could be involved in interactions with V; it is possible the exposure of these residues to solvent could be the source of heterogeneity and/or instability. The VC1 and C2 models taken together predict that the linker between C1 and C2 is 12 residues in length (Ala223 to Glu236), much larger than the 3-residue linker between V and C1. The longer linker is fully consistent with the

experimental observations showing a high degree of flexibility between C1 and C2. Hence, the overall conclusion supported by our biochemical and molecular modeling data is that V and C1 form an integrated structural unit that is fully independent of C2.

The modular structure of sRAGE differs from the initial assumption based on sequence analysis that there would be three independent domains. It has been proposed that over the course of evolution, Ig-like superfamily proteins developed a modular assembly of domains. Ideally, each domain provides unique functionality, which results in the generation of proteins that can respond to multiple ligands (56). Central to this hypothesis is the concept of one-domain, one-ligand. However, RAGE does not seem to fit this paradigm as all of its ligands identified to date, including S100B, are found to interact with the N-terminal V domain of the protein. In this respect, a recent publication suggesting S100A12 binds to the C1 domain stands out as unusual (57). However, the conclusions drawn in those studies were all based on use of a C1C2 construct with an N-terminus at Ala130. Our sequence analysis and homology modeling suggest this construct eliminates the entire first β-strand of C1, which is anticipated to be highly destabilizing. Indeed our results show that C1 does not maintain a proper fold in the absence of V. Since C1 requires V for full stability and structural integrity, the construct used in that study may well be structurally unstable and might exhibit aberrant function. The conclusion that S100A12 binds to the C1 domain may need to be re-examined with alternate reagents with these issues in mind.

The nM dissociation constant (K_D) determined for S100B binding to sRAGE and VC1 is consistent with values published for other sRAGE ligands. Dissociation constants of 60 nM, 6.4 nM, 56.8 nM, and 91 nM have been reported for AGE-BSA, amphoterin (HMG1), amyloid-β peptide, and EN-RAGE (S100A12) respectively (2,11,12,58). Recently, Wilder and coworkers showed binding of a peptide from the V domain (42–59) to S100B and reported a K_D of 11 μM (59). Notably, that result is 2–3 orders of magnitude weaker than the K_Ds for other RAGE ligands. The authors proposed an important role for Trp51 in sRAGE for binding of S100B (59). In our homology model of VC1 this residue is buried in the hydrophobic core (Figure 6A), which implies it is not involved in S100B binding. The model predicts residues adjacent to Trp51 that are part of one or more loops are much more likely to contribute to S100B-RAGE binding. This hypothesis is consistent with our results on the binding of S100B to the V domain, which revealed K_Ds of 550 nM and 470 nM. Although clearly weaker than the affinity for VC1 and sRAGE, binding of the V domain is much stronger than for the V (42–59) peptide. Nonetheless, the constructs based on V alone lack critical binding elements relative to VC1, which weakens the interaction with S100B.

Native RAGE is N-glycosylated at two potential sites in the V domain, but the bacterially expressed proteins are not glycosylated. Favorable effects from glycosylation on solubility and stability are anticipated, but the effect on the structure of folded proteins is generally believed to be quite small. There is significant evidence in support of the latter in the case of RAGE. First, RAGE can be readily deglycosylated with PNGaseF. This indicates that the carbohydrates are solvent accessible, which in turn implies they do not interact significantly with, or alter the structure of, the folded protein domains (60). Second these authors showed that RAGE deglycosylation has a minimal effect on binding of the ligands amphoterin and AGE-BSA. Third, similar observations have been recently reported for the bacterially expressed protein (37). Thus, the accumulated evidence supports the notion that our constructs serve as valid models for the study of sRAGE structure and ligand binding.

Implications for RAGE signaling

The characteristics of sRAGE structure relate to its mechanism of signaling. Our results show that the C2 domain of RAGE has significant rotational freedom from the VC1 region. Specifically, NMR spectra of sRAGE-S100B complexes show C2 is flexibly attached to VC1

and remains unperturbed when S100B binds to VC1 suggesting there is no signal passed directly between VC1 and C2. Hence, a mechanism where ligand binding in the VC1 region is transduced via C2 and the transmembrane helix to the intracellular domain is not anticipated for RAGE.

RAGE belongs to a class of receptors that contain a single transmembrane helix and signal through kinases. While most of these receptors dimerize, the degree of oligomerization varies for different members of this class. In the case of the erythropoietin receptor (EPOR), the D1 and D2 form an integrated structure that dimerizes in an autoinhibitory orientation. Ligand binding causes a conformational change in the interdomain angle, which is believed to promote signaling by enabling trans-phosphoryation of the kinases bound to the intracellular domain (61,62). The growth hormone receptor (GHR) also exists in an autoinhibited state but dimerizes via its transmembrane helix. Ligand binding to GHR results in rotation of the transmembrane helix, which in turn is transmitted to the intracellular domain because all of the structural elements are coupled (63). Thus, ligand binding causes reorientation into an architecture where trans-phosphorylation can occur. The flexibility between the VC1 and C2 domains implies neither of these allosteric mechanisms could be operative in the case of RAGE.

Signaling via RAGE occurs through the ERK1/2 kinase. Remarkably, the intracellular region of RAGE is very small and characterization of this region by CD and NMR showed it has little persistent secondary or tertiary structure (Figure S9). Despite being so small and unstructured, this domain binds to both phosphorylated and unphosphorylated ERK1/2 in a *ligand-dependent manner* (64). The absence of any structure in the intracellular domain implies the most likely mechanism for RAGE signaling is via ligand-induced oligomerization and resultant localization of multiple kinase molecules. A proposal for RAGE signaling through oligomerization has been reported based on the crystal structure of S100A12 (35). In this model three dimers (six subunits) of S100A12 bind three molecules of RAGE, but the mechanistic implications for RAGE are not described.

Figure 9 shows schematic diagrams of simple models for RAGE signaling that incorporate the multi-ligand functionality of RAGE, receptor oligomerization, and the flexibility of the C1-C2 linker. In particular, free rotation around the C1-C2 linker allows the VC1 domains to utilize different surfaces to interact with different ligands without disrupting the orientation of the signaling components (C2, transmembrane helix, and/or intracellular domain). Figure 9A shows two hypothetical signaling complexes where ligand-induced dimerization occurs on different VC1 surfaces. In this scenario, unliganded RAGE would be autoinhibited, perhaps due to electrostatic repulsion of the highly charged intracellular kinase binding domains. Ligand binding dimerizes the receptor and increases localization of ERK1/2 to initiate the signaling cascade. This model could also be adapted if it turns out that RAGE dimerizes via the transmembrane helix (or via as yet uncharacterized ligands). Figure 9B shows a schematic diagram of one such scenario where ligand binding leads to formation of a network of RAGE receptors. One important feature of this model is the VC1 domains would still have rotational freedom to present different binding surfaces for different ligands. Thus, a ligand-induced network of RAGE receptors is formed, increasing the localization of ERK1/2 to promote signaling.

Our data and observations in the literature such as the analytical ultracentrifugation study by Wilton and co-workers (37) strongly suggest the sRAGE molecule in isolation is monomeric. These results in turn point strongly to a ligand-mediated oligomerization mechanism for RAGE signaling. This hypothesis is supported by data from a variety of RAGE splice variants including a variant lacking the intracellular domain, which was found to be dominant-negative in vivo (22,40). Another splice variant lacking a portion of the V-domain was not dominant-negative, presumably because ligand binding was weakened but not abolished (65).

Determination of the oligomeric states of sRAGE-ligand complexes and the natural oligomeric state of the unliganded full receptor will be required in order to develop an understanding of the molecular basis for RAGE signaling.

Supplementary Material

Refer to Web version on PubMed Central for supplementary material.

Acknowledgements

References

1. Neeper M, Schmidt AM, Brett J, Yan SD, Wang F, Pan YC, Elliston K, Stern D, Shaw A. Cloning and expression of a cell surface receptor for advanced glycosylation end products of proteins. Journal of Biological Chemistry 1992;267:14998–15004. [PubMed: 1378843]

2. Schmidt AM, Vianna M, Gerlach M, Brett J, Ryan J, Kao J, Esposito C, Hegarty H, Hurley W, Clauss M. Isolation and characterization of two binding proteins for advanced glycosylation end products from bovine lung which are present on the endothelial cell surface. Journal of Biological Chemistry 1992;267:14987–14997. [PubMed: 1321822]

3. Yan SD, Schmidt AM, Anderson GM, Zhang J, Brett J, Zou YS, Pinsky D, Stern D. Enhanced cellular oxidant stress by the interaction of advanced glycation end products with their receptors/binding proteins. Journal of Biological Chemistry 1994;269:9889–9897. [PubMed: 8144582]

4. Schmidt AM, Hori O, Brett J, Yan SD, Wautier JL, Stern D. Cellular receptors for advanced glycation end products. Implications for induction of oxidant stress and cellular dysfunction in the pathogenesis of vascular lesions. Arteriosclerosis & Thrombosis 1994;14:1521–1528. [PubMed: 7918300]

5. Hori O, Yan SD, Ogawa S, Kuwabara K, Matsumoto M, Stern D, Schmidt AM. The receptor for advanced glycation end-products has a central role in mediating the effects of advanced glycation end-products on the development of vascular disease in diabetes mellitus. Nephrology Dialysis Transplantation 11 Suppl 1996;5:13–16.

6. Schmidt AM, Hori O, Chen JX, Li JF, Crandall J, Zhang J, Cao R, Yan SD, Brett J, Stern D. Advanced glycation endproducts interacting with their endothelial receptor induce expression of vascular cell adhesion molecule-1 (VCAM-1) in cultured human endothelial cells and in mice. A potential mechanism for the accelerated vasculopathy of diabetes. Journal of Clinical Investigation 1995;96:1395–1403. [PubMed: 7544803]

7. Ikeda K, Higashi T, Sano H, Jinnouchi Y, Yoshida M, Araki T, Ueda S, Horiuchi S. N (epsilon)-(carboxymethyl)lysine protein adduct is a major immunological epitope in proteins modified with advanced glycation end products of the Maillard reaction. Biochemistry 1996;35:8075–8083. [PubMed: 8672512]

8. Schmidt AM, Yan SD, Yan SF, Stern DM. The biology of the receptor for advanced glycation end products and its ligands. Biochimica et Biophysica Acta 2000;1498:99–111. [PubMed: 11108954]

9. Du Yan S, Zhu H, Fu J, Yan SF, Roher A, Tourtellotte WW, Rajavashisth T, Chen X, Godman GC, Stern D, Schmidt AM. Amyloid-beta peptide-receptor for advanced glycation endproduct interaction elicits neuronal expression of macrophage-colony stimulating factor: a proinflammatory pathway in Alzheimer disease. Proceedings of the National Academy of Sciences of the United States of America 1997;94:5296–5301. [PubMed: 9144231]

10. Miyata T, Hori O, Zhang J, Yan SD, Ferran L, Iida Y, Schmidt AM. The receptor for advanced glycation end products (RAGE) is a central mediator of the interaction of AGE-beta2microglobulin with human mononuclear phagocytes via an oxidant-sensitive pathway. Implications for the

pathogenesis of dialysis-related amyloidosis. Journal of Clinical Investigation 1996;98:1088–1094. [PubMed: 8787669]

11. Hori O, Brett J, Slattery T, Cao R, Zhang J, Chen JX, Nagashima M, Lundh ER, Vijay S, Nitecki D. The receptor for advanced glycation end products (RAGE) is a cellular binding site for amphoterin. Mediation of neurite outgrowth and co-expression of rage and amphoterin in the developing nervous system. Journal of Biological Chemistry 1995;270:25752–25761. [PubMed: 7592757]

12. Hofmann MA, Drury S, Fu C, Qu W, Taguchi A, Lu Y, Avila C, Kambham N, Bierhaus A, Nawroth P, Neurath MF, Slattery T, Beach D, McClary J, Nagashima M, Morser J, Stern D, Schmidt AM. RAGE mediates a novel proinflammatory axis: a central cell surface receptor for S100/calgranulin polypeptides. Cell 1999;97:889–901. [PubMed: 10399917]

13. Arumugam T, Simeone DM, Schmidt AM, Logsdon CD. S100P stimulates cell proliferation and survival via receptor for activated glycation end products (RAGE). Journal of Biological Chemistry 2004;279:5059–5065. [PubMed: 14617629]

14. Sorci G, Riuzzi F, Agneletti AL, Marchetti C, Donato R. S100B inhibits myogenic differentiation and myotube formation in a RAGE-independent manner. Molecular & Cellular Biology 2003;23:4870–4881. [PubMed: 12832473]

15. Yamagishi S, Adachi H, Nakamura K, Matsui T, Jinnouchi Y, Takenaka K, Takeuchi M, Enomoto M, Furuki K, Hino A, Shigeto Y, Imaizumi T. Positive association between serum levels of advanced glycation end products and the soluble form of receptor for advanced glycation end products in nondiabetic subjects. Metabolism 2006;55:1227–1231. [PubMed: 16919543]

16. Koyama H, Shoji T, Yokoyama H, Motoyama K, Mori K, Fukumoto S, Emoto M, Tamei H, Matsuki H, Sakurai S, Yamamoto Y, Yonekura H, Watanabe T, Yamamoto H, Nishizawa Y. Plasma level of endogenous secretory RAGE is associated with components of the metabolic syndrome and atherosclerosis. Arteriosclerosis, Thrombosis & Vascular Biology 2005;25:2587–2593.

17. Stern DM, Yan SD, Yan SF, Schmidt AM. Receptor for advanced glycation endproducts (RAGE) and the complications of diabetes. Ageing Res Rev 2002;1:1–15. [PubMed: 12039445]

18. Stern D, Yan SD, Yan SF, Schmidt AM. Receptor for advanced glycation endproducts: a multiligand receptor magnifying cell stress in diverse pathologic settings. Advanced Drug Delivery Reviews 2002;54:1615–1625. [PubMed: 12453678]

19. Yamagishi S, Takeuchi M, Inagaki Y, Nakamura K, Imaizumi T. Role of advanced glycation end products (AGEs) and their receptor (RAGE) in the pathogenesis of diabetic microangiopathy. International Journal of Clinical Pharmacology Research 2003;23:129–134. [PubMed: 15224502]

20. Rauvala H, Merenmies J, Pihlaskari R, Korkolainen M, Huhtala ML, Panula P. The adhesive and neurite-promoting molecule p30: analysis of the amino-terminal sequence and production of antipeptide antibodies that detect p30 at the surface of neuroblastoma cells and of brain neurons. Journal of Cell Biology 1988;107:2293–2305. [PubMed: 2461949]

21. Heizmann CW, Fritz G, Schafer BW. S100 proteins: structure, functions and pathology. Frontiers in Bioscience 2002;7:d1356–1368. [PubMed: 11991838]

22. Fages C, Nolo R, Huttunen HJ, Eskelinen E, Rauvala H. Regulation of cell migration by amphoterin. Journal of Cell Science 2000;113:611–620. [PubMed: 10652254]

23. Huttunen HJ, Kuja-Panula J, Sorci G, Agneletti AL, Donato R, Rauvala H. Coregulation of neurite outgrowth and cell survival by amphoterin and S100 proteins through receptor for advanced glycation end products (RAGE) activation. Journal of Biological Chemistry 2000;275:40096–40105. [PubMed: 11007787]

24. Taguchi A, Blood DC, del Toro G, Canet A, Lee DC, Qu W, Tanji N, Lu Y, Lalla E, Fu C, Hofmann MA, Kislinger T, Ingram M, Lu A, Tanaka H, Hori O, Ogawa S, Stern DM, Schmidt AM. Blockade of RAGE-amphoterin signalling suppresses tumour growth and metastases, [see comment]. Nature 2000;405:354–360. [PubMed: 10830965]

25. Park L, Raman KG, Lee KJ, Lu Y, Ferran LJ Jr, Chow WS, Stern D, Schmidt AM. Suppression of accelerated diabetic atherosclerosis by the soluble receptor for advanced glycation endproducts. Nat Med 1998;4:1025–1031. [PubMed: 9734395]

26. Hudson BI, Schmidt AM. RAGE: a novel target for drug intervention in diabetic vascular disease. Pharmaceutical Research 2004;21:1079–1086. [PubMed: 15290845]

27. Schmidt AM, Stern DM. RAGE: a new target for the prevention and treatment of the vascular and inflammatory complications of diabetes. Trends Endocrinol Metab 2000;11:368–375. [PubMed: 11042467]

28. Hudson BI, Bucciarelli LG, Wendt T, Sakaguchi T, Lalla E, Qu W, Lu Y, Lee L, Stern DM, Naka Y, Ramasamy R, Yan SD, Yan SF, D'Agati V, Schmidt AM. Blockade of receptor for advanced glycation endproducts: a new target for therapeutic intervention in diabetic complications and inflammatory disorders. Archives of Biochemistry & Biophysics 2003;419:80–88. [PubMed: 14568011]

29. Davey GE, Murmann P, Heizmann CW. Intracellular Ca2+ and Zn2+ levels regulate the alternative cell density-dependent secretion of S100B in human glioblastoma cells. J Biol Chem 2001;276:30819–30826. [PubMed: 11402046]

30. Rintala-Dempsey AC, Santamaria-Kisiel L, Liao Y, Lajoie G, Shaw GS. Insights into S100 target specificity examined by a new interaction between S100A11 and annexin A2. Biochemistry 2006;45:14695–14705. [PubMed: 17144662]

31. Sastry M, Ketchem RR, Crescenzi O, Weber C, Lubienski MJ, Hidaka H, Chazin WJ. The three-dimensional structure of Ca(2+)-bound calcyclin: implications for Ca(2+)-signal transduction by S100 proteins. Structure 1998;6:223–231. [PubMed: 9519412]

32. Maler L, Sastry M, Chazin WJ. A structural basis for S100 protein specificity derived from comparative analysis of apo and Ca(2+)-calcyclin. Journal of Molecular Biology 2002;317:279–290. [PubMed: 11902843]

33. Deloulme JC, Gentil BJ, Baudier J. Monitoring of S100 homodimerization and heterodimeric interactions by the yeast two-hybrid system. Microscopy Research & Technique 2003;60:560–568. [PubMed: 12645004]

34. Itou H, Yao M, Fujita I, Watanabe N, Suzuki M, Nishihira J, Tanaka I. The crystal structure of human MRP14 (S100A9), a Ca(2+)-dependent regulator protein in inflammatory process. Journal of Molecular Biology 2002;316:265–276. [PubMed: 11851337]

35. Moroz OV, Antson AA, Dodson EJ, Burrell HJ, Grist SJ, Lloyd RM, Maitland NJ, Dodson GG, Wilson KS, Lukanidin E, Bronstein IB. The structure of S100A12 in a hexameric form and its proposed role in receptor signalling. Acta Crystallographica Section D-Biological Crystallography 2002;58:407–413.

36. Machius M, Cianga P, Deisenhofer J, Ward ES. Crystal structure of a T cell receptor Valpha11 (AV11S5) domain: new canonical forms for the first and second complementarity determining regions. Journal of Molecular Biology 2001;310:689–698. [PubMed: 11453680]

37. Wilton R, Yousef MA, Saxena P, Szpunar M, Stevens FJ. Expression and purification of recombinant human receptor for advanced glycation endproducts in Escherichia coli. Protein Expression and Purification 2006;47:25–35. [PubMed: 16510295]

38. Hanford LE, Enghild JJ, Valnickova Z, Petersen SV, Schaefer LM, Schaefer TM, Reinhart TA, Oury TD. Purification and characterization of mouse soluble receptor for advanced glycation end products (sRAGE). Journal of Biological Chemistry 2004;279:50019–50024. [PubMed: 15381690]

39. Ostendorp T, Weibel M, Leclerc E, Kleinert P, Kroneck PM, Heizmann CW, Fritz G. Expression and purification of the soluble isoform of human receptor for advanced glycation end products (sRAGE) from Pichia pastoris. Biochemical & Biophysical Research Communications 2006;347:4–11. [PubMed: 16806067]

40. Huttunen HJ, Fages C, Rauvala H. Receptor for advanced glycation end products (RAGE)-mediated neurite outgrowth and activation of NF-kappaB require the cytoplasmic domain of the receptor but different downstream signaling pathways. Journal of Biological Chemistry 1999;274:19919–19924. [PubMed: 10391939]

41. Bork P, Holm L, Sander C. The immunoglobulin fold. Structural classification, sequence patterns and common core. Journal of Molecular Biology 1994;242:309–320. [PubMed: 7932691]

42. Ostendorp T, Heizmann CW, Kroneck PM, Fritz G. Purification, crystallization and preliminary X-ray diffraction studies on human Ca2+-binding protein S100B. Acta Crystallograph Sect F Struct Biol Cryst Commun 2005;61:673–675.

43. Andrade MA, Chacon P, Merelo JJ, Moran F. Evaluation of secondary structure of proteins from UV circular dichroism spectra using an unsupervised learning neural network. Protein Eng 1993;6:383–390. [PubMed: 8332596]

44. Johnsson B, Lofas S, Lindquist G. Immobilization of proteins to a carboxymethyldextran-modified gold surface for biospecific interaction analysis in surface plasmon resonance sensors. Analytical Biochemistry 1991;198:268–277. [PubMed: 1724720]

45. Myszka DG. Improving biosensor analysis. Journal of Molecular Recognition 1999;12:279–284. [PubMed: 10556875]

46. Roden LD, Myszka DG. Global analysis of a macromolecular interaction measured on BIAcore. Biochemical & Biophysical Research Communications 1996;225:1073–1077. [PubMed: 8780736]

47. Pervushin K, Riek R, Wider G, Wuthrich K. Attenuated T2 relaxation by mutual cancellation of dipole-dipole coupling and chemical shift anisotropy indicates an avenue to NMR structures of very large biological macromolecules in solution. Proceedings of the National Academy of Sciences of the United States of America 1997;94:12366–12371. [PubMed: 9356455]

48. Bartels C, Xia T, Billeter M, Guntert P, Wuthrich K. The program XEASY for computer-supported NMR spectral analysis of biological macromolecules. Journal of Biomolecular NMR 1995;6:1–10.

49. Lambert C, Leonard N, De Bolle X, Depiereux E. ESyPred3D: Prediction of proteins 3D structures. Bioinformatics 2002;18:1250–1256. [PubMed: 12217917]

50. Canutescu AA, Shelenkov AA, Dunbrack RL Jr. A graph-theory algorithm for rapid protein side-chain prediction. Protein Sci 2003;12:2001–2014. [PubMed: 12930999]

51. Morris AL, MacArthur MW, Hutchinson EG, Thornton JM. Stereochemical quality of protein structure coordinates. Proteins 1992;12:345–364. [PubMed: 1579569]

52. Renard C, Chappey O, Wautier MP, Nagashima M, Lundh E, Morser J, Zhao L, Schmidt AM, Scherrmann JM, Wautier JL. Recombinant advanced glycation end product receptor pharmacokinetics in normal and diabetic rats. Molecular Pharmacology 1997;52:54–62. [PubMed: 9224812]

53. Chung CM, Chiu JD, Connors LH, Gursky O, Lim A, Dykstra AB, Liepnieks J, Benson MD, Costello CE, Skinner M, Walsh MT. Thermodynamic stability of a kappaI immunoglobulin light chain: relevance to multiple myeloma. Biophys J 2005;88:4232–4242. [PubMed: 15792972]

54. Eletsky A, Kienhofer A, Pervushin K. TROSY NMR with partially deuterated proteins. Journal of Biomolecular NMR 2001;20:177–180. [PubMed: 11495249]

55. Koppal T, Lam AG, Guo L, Van Eldik LJ. S100B proteins that lack one or both cysteine residues can induce inflammatory responses in astrocytes and microglia. Neurochemistry International 2001;39:401–407. [PubMed: 11578775]

56. Haspel J, Grumet M. The L1CAM extracellular region: a multi-domain protein with modular and cooperative binding modes. Frontiers in Bioscience 2003;8:s1210–1225. [PubMed: 12957823]

57. Xie J, Burz DS, He W, Bronstein IB, Lednev IK, Shekhtman A. Hexameric calgranulin C (S100A12) binds to the receptor for advanced glycated end products (RAGE) using symmetric hydrophobic target-binding patches. J Biol Chem. 2006

58. Yan SD, Chen X, Fu J, Chen M, Zhu H, Roher A, Slattery T, Zhao L, Nagashima M, Morser J, Migheli A, Nawroth P, Stern D, Schmidt AM. RAGE and amyloid-beta peptide neurotoxicity in Alzheimer's disease. [see comment]. Nature 1996;382:685–691. [PubMed: 8751438]

59. Wilder PT, Lin J, Bair CL, Charpentier TH, Yang D, Liriano M, Varney KM, Lee A, Oppenheim AB, Adhya S, Carrier F, Weber DJ. Recognition of the tumor suppressor protein p53 and other protein targets by the calcium-binding protein S100B. Biochim Biophys Acta. 2006

60. Srikrishna G, Huttunen HJ, Johansson L, Weigle B, Yamaguchi Y, Rauvala H, Freeze HH. N-Glycans on the receptor for advanced glycation end products influence amphoterin binding and neurite outgrowth. Journal of Neurochemistry 2002;80:998–1008. [PubMed: 11953450]

61. Livnah O, Stura EA, Middleton SA, Johnson DL, Jolliffe LK, Wilson IA. Crystallographic evidence for preformed dimers of erythropoietin receptor before ligand activation. Science 1999;283:987–990. [PubMed: 9974392]

62. Syed RS, Reid SW, Li C, Cheetham JC, Aoki KH, Liu B, Zhan H, Osslund TD, Chirino AJ, Zhang J, Finer-Moore J, Elliott S, Sitney K, Katz BA, Matthews DJ, Wendoloski JJ, Egrie J, Stroud RM.

Efficiency of signalling through cytokine receptors depends critically on receptor orientation. Nature 1998;395:511–516. [PubMed: 9774108]

63. Brown RJ, Adams JJ, Pelekanos RA, Wan Y, McKinstry WJ, Palethorpe K, Seeber RM, Monks TA, Eidne KA, Parker MW, Waters MJ. Model for growth hormone receptor activation based on subunit rotation within a receptor dimer. Nat Struct Mol Biol 2005;12:814–821. [PubMed: 16116438]

64. Ishihara K, Tsutsumi K, Kawane S, Nakajima M, Kasaoka T. The receptor for advanced glycation end-products (RAGE) directly binds to ERK by a D-domain-like docking site. FEBS Letters 2003;550:107–113. [PubMed: 12935895]

65. Yonekura H, Yamamoto Y, Sakurai S, Petrova RG, Abedin MJ, Li H, Yasui K, Takeuchi M, Makita Z, Takasawa S, Okamoto H, Watanabe T, Yamamoto H. Novel splice variants of the receptor for advanced glycation end-products expressed in human vascular endothelial cells and pericytes, and their putative roles in diabetes-induced vascular injury. Biochem J 2003;370:1097–1109. [PubMed: 12495433]

66. Pettersen EF, Goddard TD, Huang CC, Couch GS, Greenblatt DM, Meng EC, Ferrin TE. UCSF Chimera--a visualization system for exploratory research and analysis. J Comput Chem 2004;25:1605–1612. [PubMed: 15264254]

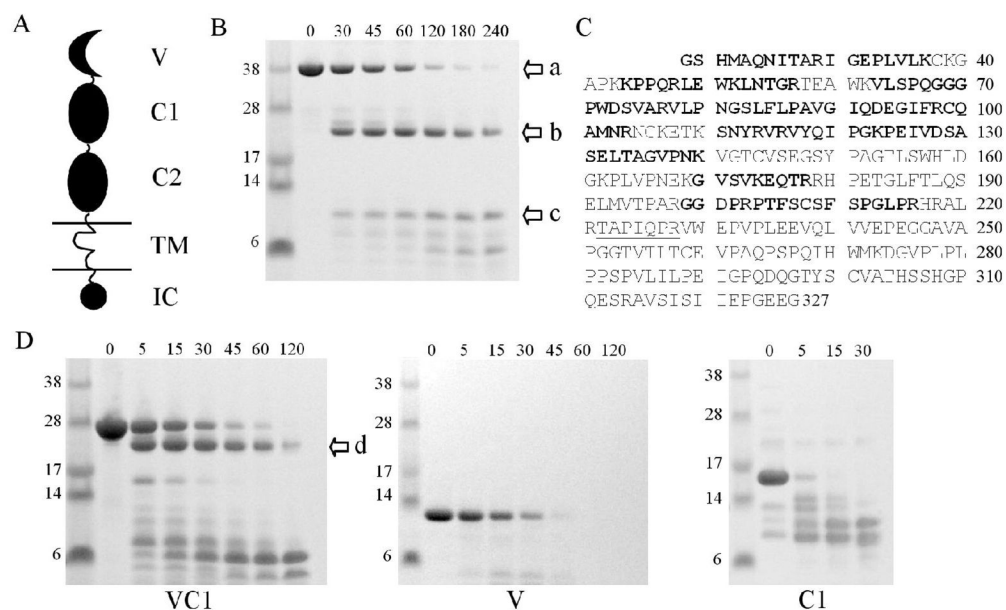**Figure 1.**
Limited proteolysis of sRAGE and domain constructs. (A) Schematic diagram of the structure of RAGE with each domain labeled. (B) Reducing SDS-PAGE of sRAGE digested by trypsin (500:1, w/w) at room temperature. Arrows at right highlight the three main fragments. Each of these bands shift in mobility when gels are run under non-reducing conditions indicating they contain one or more disulfide bonds. Time points are given in minutes. (C) Sequence of recombinant sRAGE after removal of His6-tag. The first four amino acids (GSHM) remain after thrombin cleavage. Ala23 is the first amino acid of the mature protein after the signal sequence is removed. Highlighted in bold are peptides observed in mass spectrometry analysis of the trypsinized 25 kDa band (band b) in panel (B). The only peptide observed in the mass spectrometry analysis of band a that is not seen in band b is underlined. The numbering on the right corresponds to the last amino acid in each row. (D) Reducing SDS-PAGE of VC1, V, and C1 proteolyses by trypsin (500:1, w/w). The mobility of band d and that for the intact protein shift when run under non-reducing conditions. Time points are given in minutes.
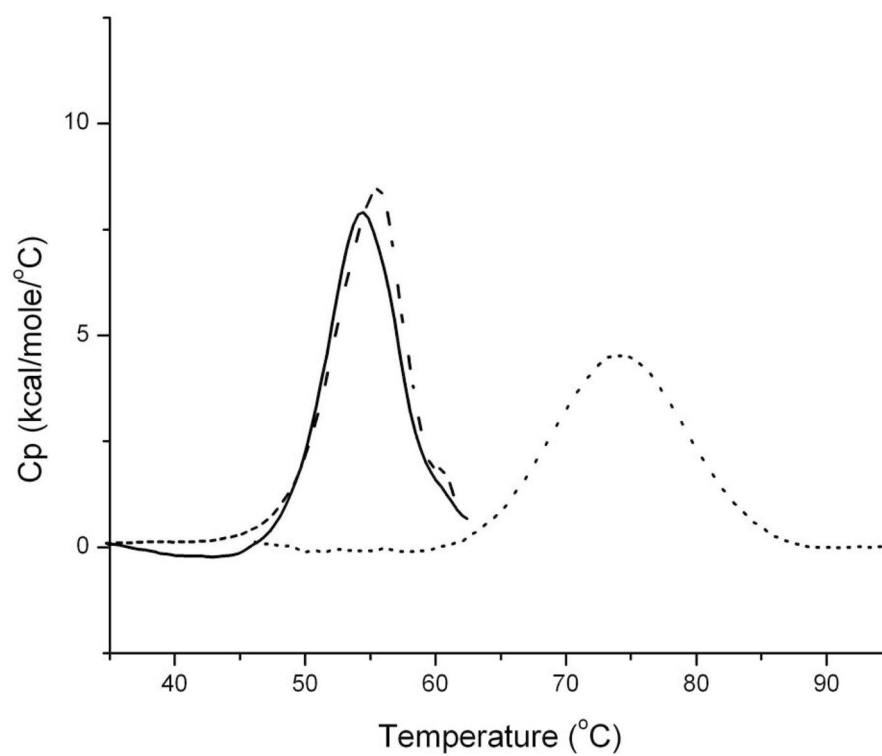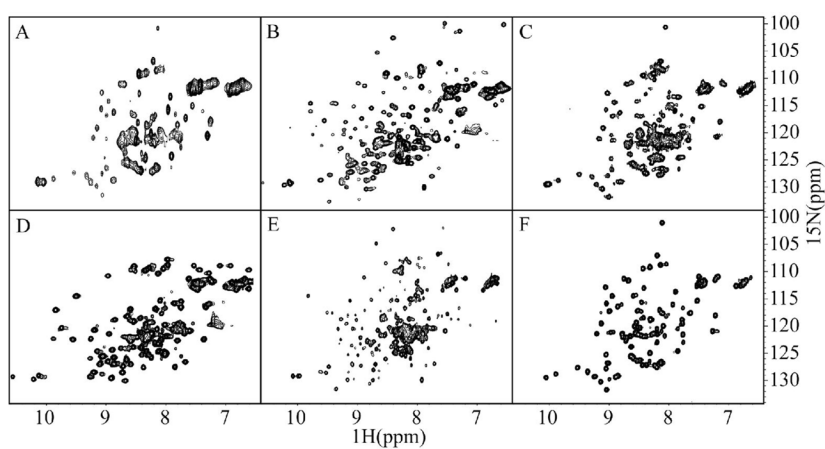
Figure 2.
Differential Scanning Calorimetry thermograms for sRAGE (–), VC1 (--) and C2 (. .).
Experiment details are provided in Methods.

Figure 3.
Heteronuclear NMR spectra of RAGE constructs. 15N-1H HSQC spectra are shown for sRAGE (A), VC1 (B), C1C2 (C), V (D), C1 (E), and C2 (F). The data were collected at 600 (C1C2, C1) or 800 (sRAGE, VC1, V, C2) MHz at 25 °C. Solution conditions are provided in Methods.
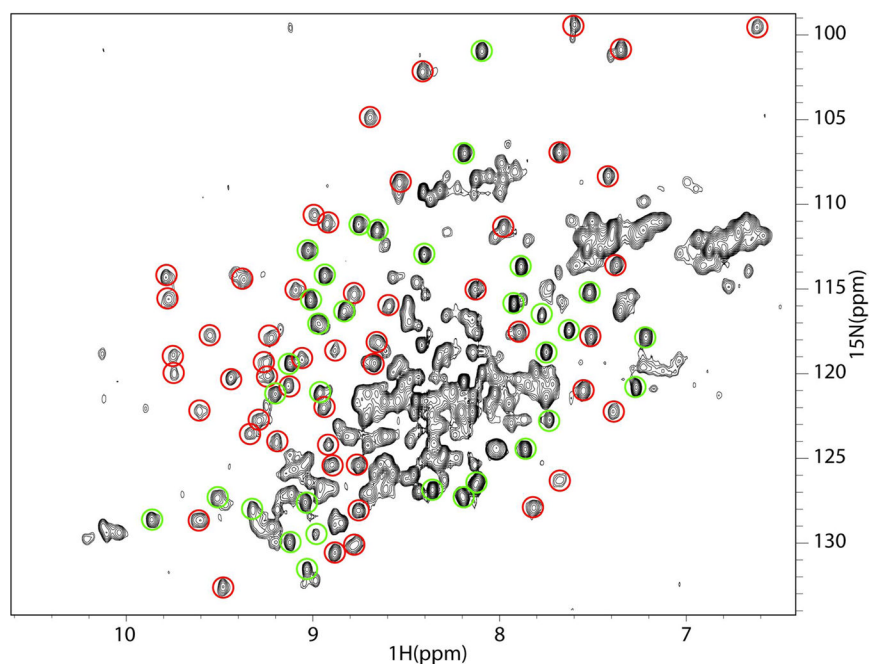
Figure 4.
Domain analysis of sRAGE using heteronuclear NMR. 15N-1H HSQC spectrum of perdeuterated sRAGE is shown with peaks labeled based on direct comparison to the spectra of VC1 and C2. Red circles denote crosspeaks uniquely assigned to VC1 and green circles denote crosspeaks uniquely assigned to C2. Unmarked crosspeaks represent those that are overlapped or are not sufficiently unique to be confidently assigned by comparison to one of the two sub-spectra.
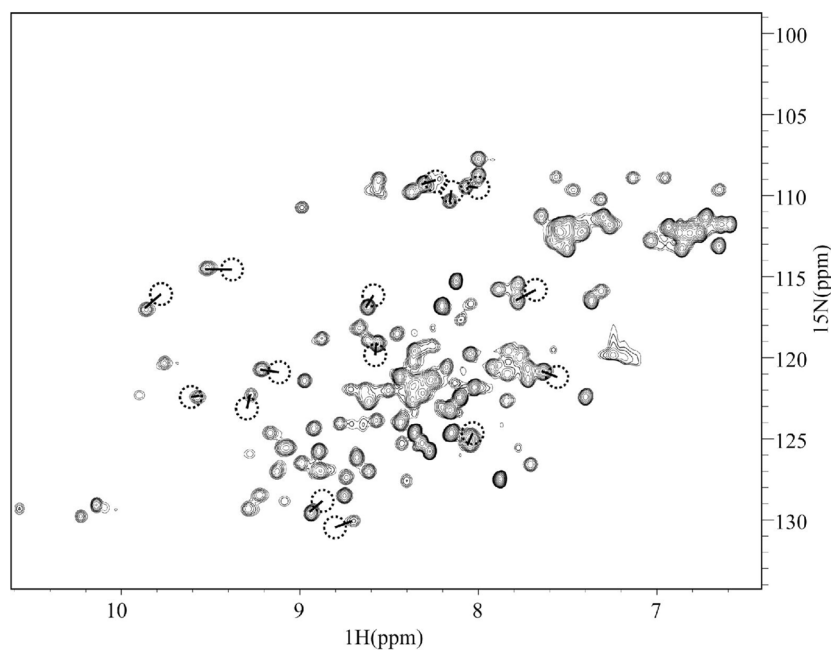
Figure 5.
Comparison of the heteronuclear NMR spectra of isolated V construct and the tandem VC1 construct. The 15N-1H HSQC spectrum of isolated V is shown with circles marking the position of same crosspeaks in the spectrum of VC1. Lines are drawn between a crosspeak in the V spectrum and the crosspeak of nearest proximity in the VC1 spectrum. Unmarked crosspeaks either do not experience significant chemical shift perturbations or cannot be analyzed due to overlap.
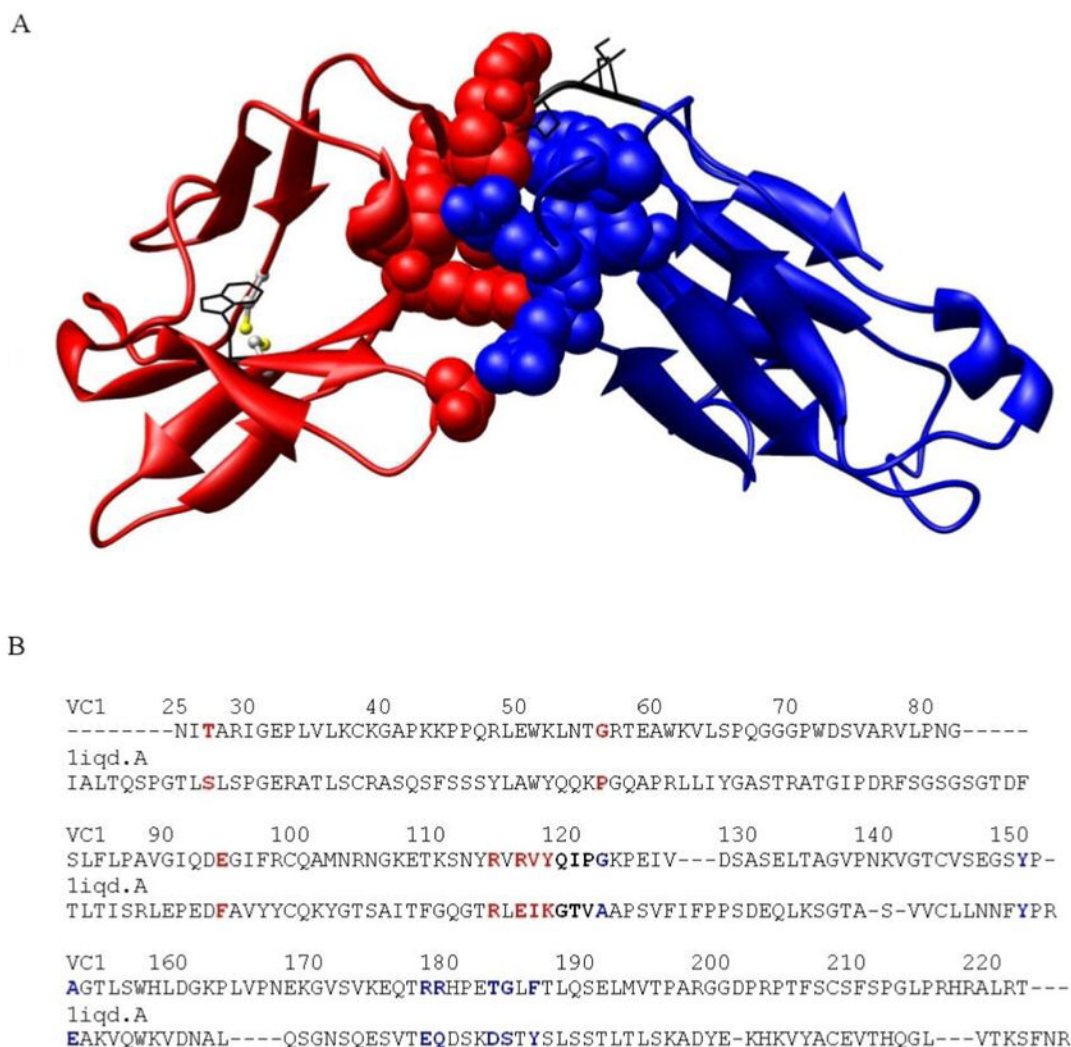
A

B

```
VC1    25   30        40        50        60        70        80
--------NITARIGEPLVLKCKGAPKKPPQRLEWKLNTGRTEAWKVLSPQGGGPWDSVARVLPNG-----
1iqd.A
IALTQSPGTLSLSPGERATLSCRASQSFSSSYLAWYQQKPGQAPRLLIYGASTRATGIPDRFSGSGSGTDF

VC1    90        100       110       120       130       140       150
SLFLPAVGIQDEGIFRCQAMNRNGKETKSNYRVRVYQIPGKPEIV---DSASELTAGVPNKVGTCVSEGSYP-
1iqd.A
TLTISRLEPEDFAVYYCQKYGTSAITFGQGTRLEIKGTVAAPSVFIFPPSDEQLKSGTA-S-VVCLLNNFYPR

VC1    160       170       180       190       200       210       220
AGTLSWHLDGKPLVPNEKGVSVKEQTRRHPETGLFTLQSELMVTPARGGDPRPTFSCSFSPGLPRHRALRT---
1iqd.A
EAKVQWKVDNAL----QSGNSQESVTEQDSKDSTYSLSSTLTLSKADYE-KHKVYACEVTHQGL---VTKSFNR
```

Figure 6.
Homology modeling of VC1. (A) Ribbon diagram of the homology model of VC1 with the V domain (25–118) shown in red, the linker (119–121) in black, and the C1 domain (122–222) in blue. Side chains for the linker residues are shown as black wires. Side chains for V and C1 involved in inter-domain packing are shown in space filling representation in the respective colors for the domains. The side chain of Trp51 is shown as black wire. The side chains for the two cysteine residues in the V domain are shown in ball and stick colored according to atom (grey, carbon; yellow, sulfur). (B) Pairwise alignment of VC1 with the A chain of PDB molecule 1IQD. Residues in the linker region are in bold. Residues involved in inter-domain packing are highlighted in the respective colors used in A (V, red; C1, blue). Figure made using Chimera (66).
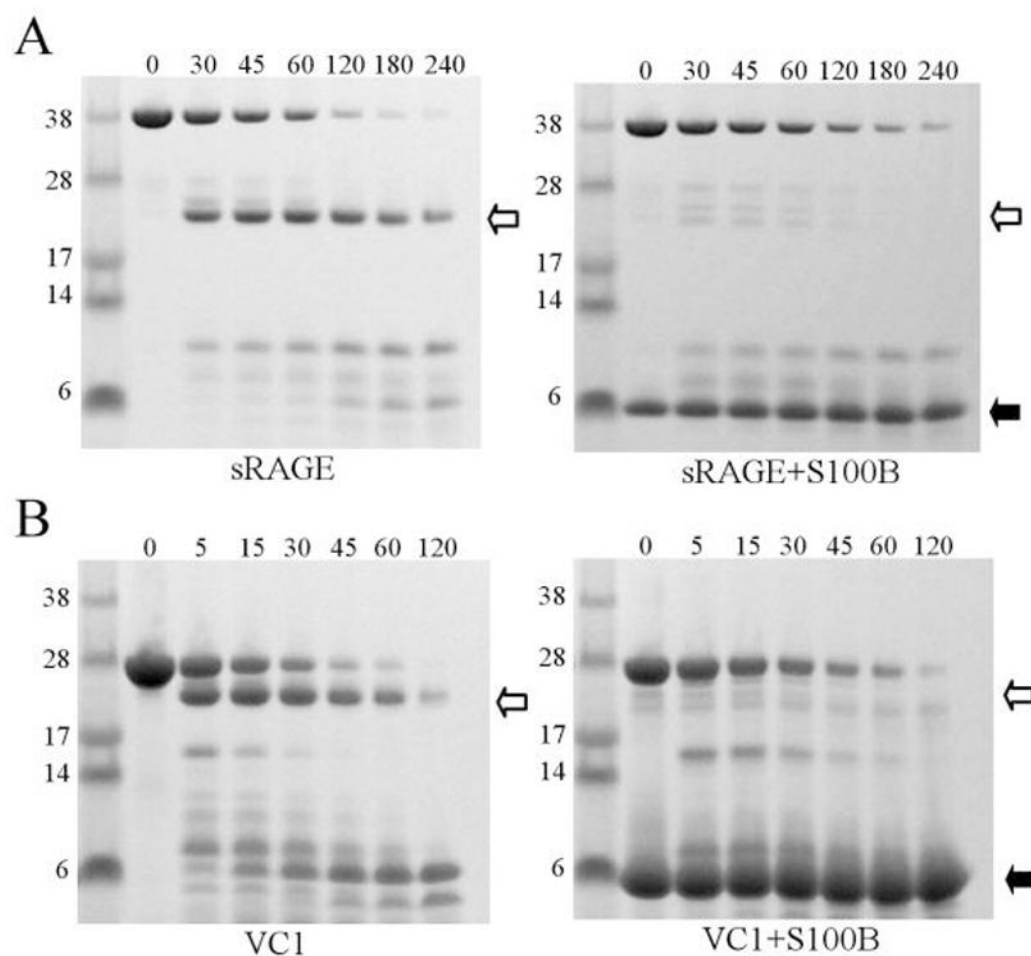
Figure 7.
Protease protection of sRAGE by Ca2+-S100B(C84S). Reducing SDS-PAGE of sRAGE (A) and VC1 (B) incubated with trypsin in the absence (left) or presence (right) of Ca2+-S100B (C84S). Solution conditions were the same in the absence and presence of S100 protein and are described in Methods. Solid arrows mark the S100B(C84S) band. Open arrows mark the stable 25 kDa VC1 fragment most affected by S100B(C84S) binding. Time points are given in minutes.
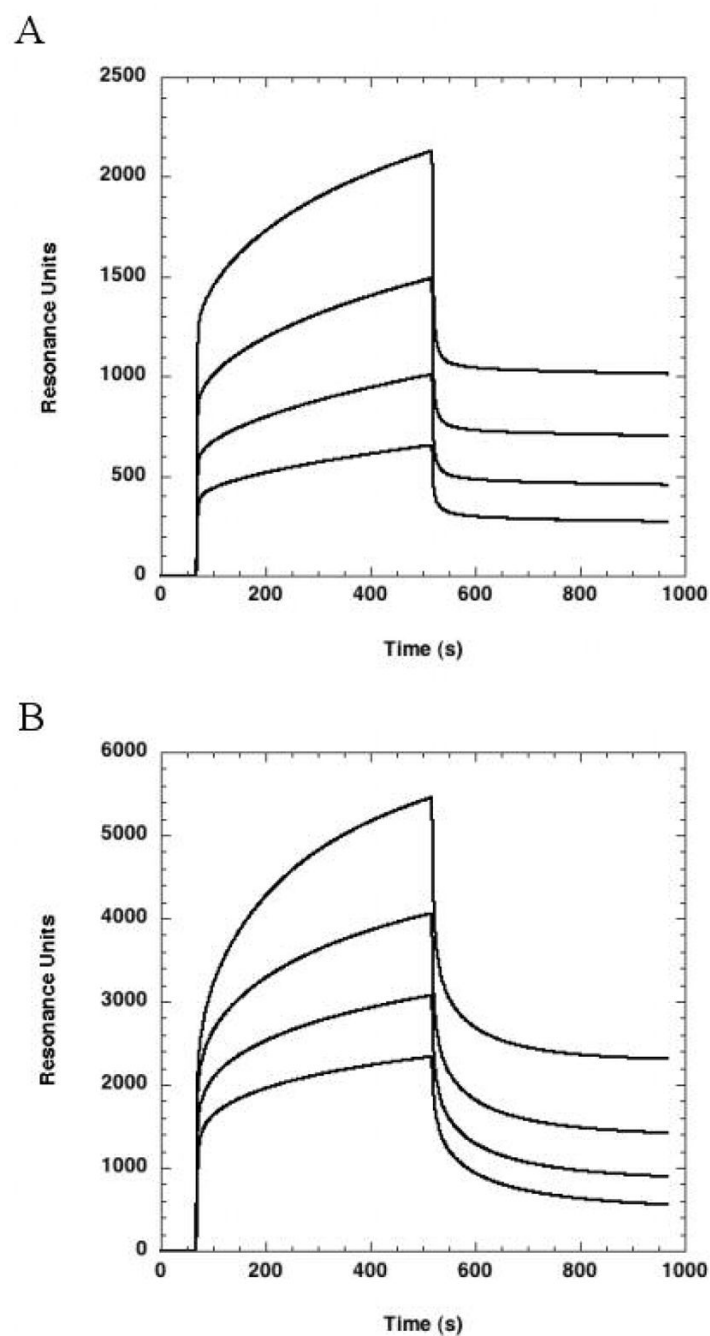
Figure 8.
SPR binding of S100B to sRAGE domains. Representative binding sensorgrams for S100B binding to (A) immobilized VC1 and (B) immobilized V. Injection concentrations from top to bottom are 12.6 μM, 6.3 μM, 3.15 μM, and 1.57 μM for both (A) and (B).
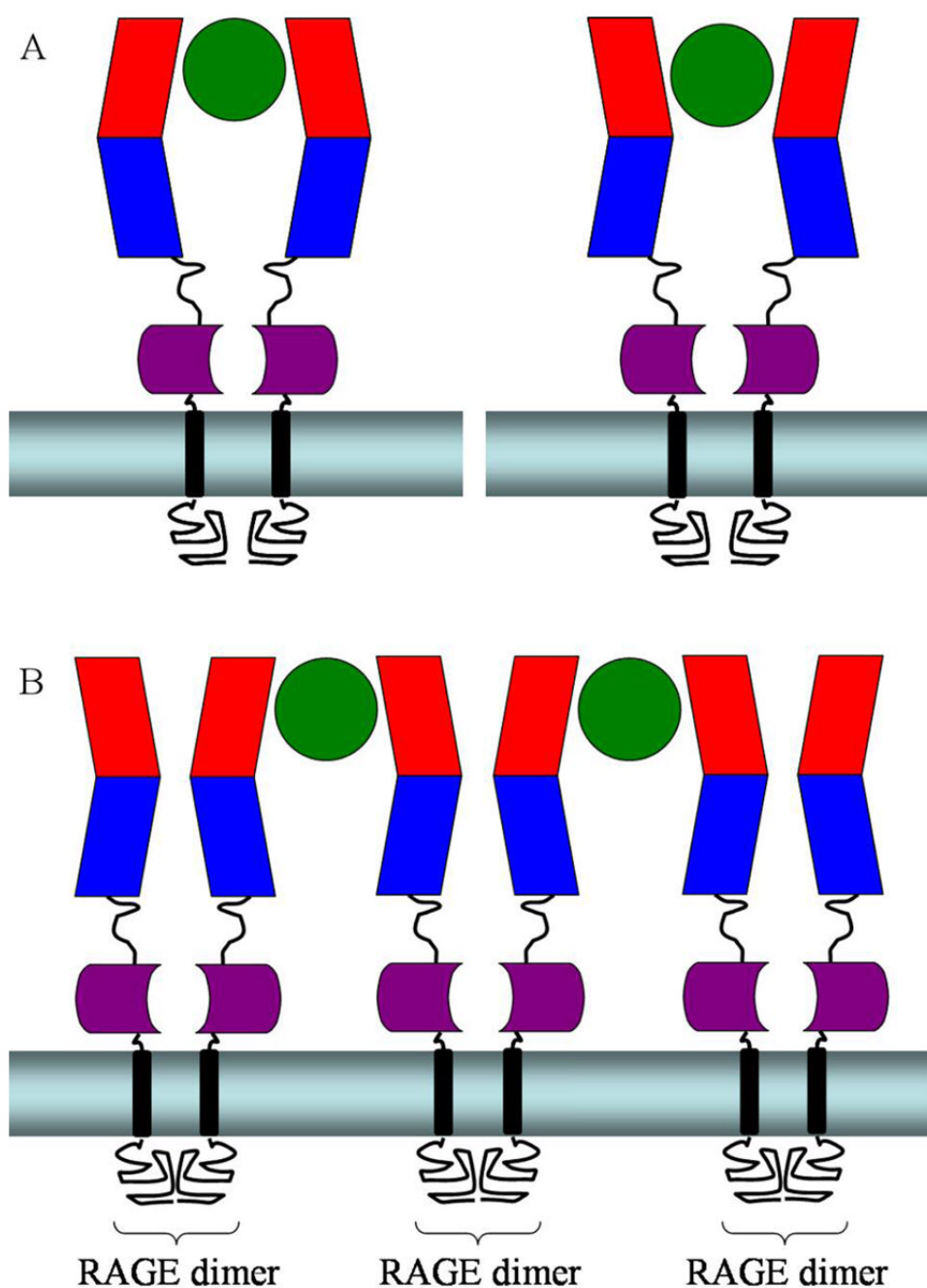
Figure 9.
Models for ligand-induced activation of RAGE through oligomerization. (A) Schematic diagram showing ligand-induced dimerization is possible using different surfaces of VC1. (B) Schematic diagram of ligand-induced network of RAGE dimers. The ligand is shown as a green circle. For Table of Contents Use Only